Journal of the Korean Astronomical Society
49: 209 ∼ 223, 2016 October

http://dx.doi.org/10.5303/JKAS.2016.49.5.209
pISSN: 1225-4614 · eISSN: 2288-890X
http://jkas.kas.org

KMTNet Supernova Program Variable Objects I. NGC 2784 Field

Matthias Yang He[1,5], Dae-Sik Moon[1], Hilding Neilson[1], Jae-Joon Lee[2], Sang Chul Kim[2,3], Mina Pak[2,3], Hong Soo Park[2,3], Dong-Jin Kim[2], Yongseok Lee[2,4], Seung-Lee Kim[2,3], and Chung-Uk Lee[2,3]

[1]Department of Astronomy and Astrophysics, University of Toronto, St. George, Toronto, ON M5S 1A1, Canada
matthias.he@mail.utoronto.ca
[2]Korea Astronomy and Space Science Institute, 776 Daedeokdae-ro, Yuseong-gu, Daejeon 34055, Korea
[3]Korea University of Science and Technology, 217 Gajeong-ro, Yuseong-gu, Daejeon 34113, Korea
[4]School of Space Research, Kyung Hee University, 1732 Deogyeongdae-ro, Giheung-gu, Yongin, Kyeonggi 17104, Korea
[5]Department of Astronomy and Astrophysics, The Pennsylvania State University, University Park, PA 16802, USA

Received September 6, 2016; accepted October 5, 2016

Abstract: We present analyses of ∼1250 variable sources identified in a 20 square degree field toward NGC 2784 by the KMTNet Supernova Program. We categorize the variable sources into three groups based on their B-band variability. The first group consists of 31 high variability sources with their B-band RMS variability greater than 0.3 magnitudes. The second group of medium variability contains 265 sources with RMS variability between 0.05 and 0.3 magnitudes. The remaining 951 sources belong to the third group of low variability with an RMS variability smaller than 0.05 magnitudes. Of the entire ∼1250 sources, 4 clearly show periods of variability greater than 100 days, while the rest have periods shorter than ∼51 days or no reliable periods. The majority of the sources show either rather irregular variability or short periods faster than 2 days. Most of the sources with reliable period determination between 2 and 51 days belong to the low-variability group, although a few belong to the medium-variability group. All the variable sources with periods longer than 35 days appear to be very red with $B-V > 1.5$ and $V-I > 2.1$ magnitudes. We classify candidates of 51 Cepheids, 17 semi-regular variables, 3 Mira types, 2 RV(B) Tauri stars, 26 eclipsing binary systems and 1 active galactic nucleus. The majority of long-term variables in our sample belong to either Mira or semi-regular types, indicating that long-term variability may be more prominent in post-main sequence phases of late-type stars. The depth of the eclipsing dips of the 26 candidates for eclipsing binaries is equivalent to ∼0.61 as the average relative size of the two stars in the binary system. Our results illustrate the power of the KMTNet Supernova Program for future studies of variable objects.

Key words: supernovae — transients — stars: variables: Cepheids — stars: binaries: eclipsing

1. Introduction

The study of variable objects in astronomy is fundamental and encompasses a wide array of sources with different physical natures. Variable objects, by definition, exhibit non-constant fluxes; thus, they include objects which appear to be variable for a number of different reasons. Some of these sources are intrinsically variable while others vary because of their orientation to the observer. For example, a pulsating or exploding star can exhibit substantial variability due to its intrinsic physical phenomena, whereas an eclipse of an object by another object leads to variability owing to their geometrical orientation with respect to an observer.

Intrinsic variable signatures often arise in objects with inherently fluctuating profiles and/or more extreme phenomena. Some stars have very long periods of variability, where the pulsation can last several hundred days and cause differences of several magnitudes in brightness–Mira type and Cepheid variables are such examples of long-period variability. There are other variable stars with short periods less than one day such as the RR Lyrae and δ Scuti stars. They provide important clues for the understanding of the internal structure of late type stars along with their evolution (Cox 1980; Percy 2007). Cepheids vary with periods of a few to about one hundred days. Empirically it has been determined that longer periods correspond to higher intrinsic brightnesses (Leavitt & Pickering 1912). The reliability of this relation makes them excellent standard candles for distance determination and contribute to the determination of the age of the Universe (Hubble 1929; Freedman et al. 2001; Freedman & Madore 2010; Riess et al. 2016). More abrupt variabilities have been observed, including novae, supernovae and gamma-ray bursts which are of great importance and interest in modern astronomy, including the identification of the accelerated expansion of the Universe (Perlmutter et al. 1998).

Variability caused by geometrical configuration of two objects are, on the other hand, usually from eclipsing binaries and transiting exoplanetary systems. It is estimated that at least half of all stars are in binary

Corresponding author: M. Y. He

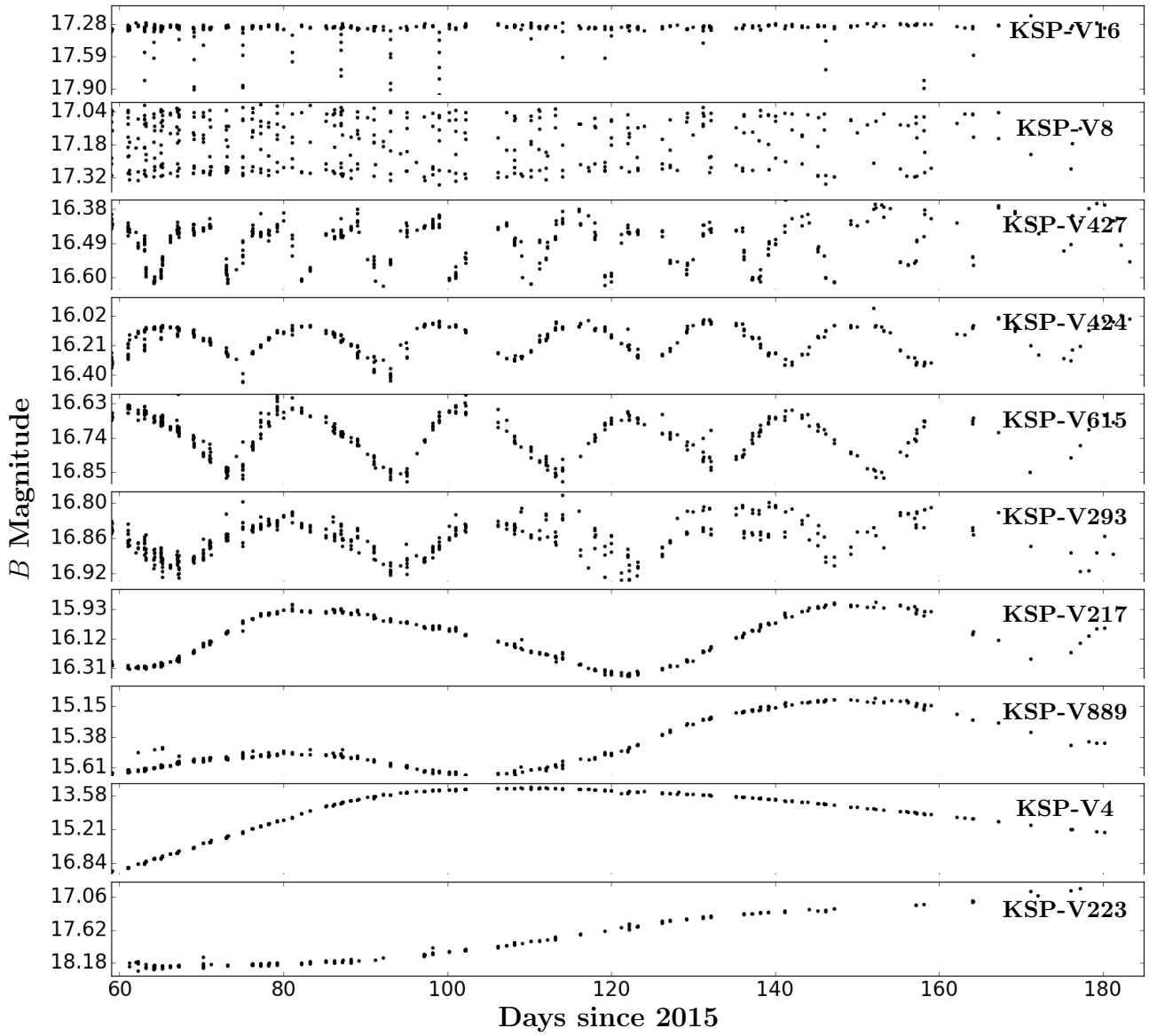

Figure 1. Sample of variable light curves in the B filter. We use the following acronyms for the different types of the variables: CEP for Cepheid, SR for semi-regular, M for Mira, RV(B) for RV(B) Tauri, E for eclipsing binary, AGN for active galactic nucleus, and S for unstudied. From top to bottom, their details (classification - refer to Section 4 for their explanations, B band RMS variability, period) are as follows: KSP-V16 (E, 0.116 magnitudes, unknown); KSP-V8 (S, 0.102 magnitudes, unknown); KSP-V427 (CEP, 0.069 magnitudes, 9.2 days); KSP-V424 (CEP, 0.097 magnitudes, 16.8 days); KSP-V615 (CEP, 0.067 magnitudes, 20.2 days); KSP-V293 (CEP, 0.031 magnitudes, 25.3 days); KSP-V217 (SR, 0.146 magnitudes, 50.6 days); KSP-V889 (SR, 0.168 magnitudes, unknown); KSP-V4 (M, 1.275 magnitudes, $\sim$150 days); and KSP-V223 (M, 0.372 magnitudes, $>$150 days).

pairs (Percy 2007), with only a small fraction of those actually in an eclipsing configuration. Eclipsing variables, in most cases, involve two stars in close proximity since a smaller separation gives a greater probability that the stars will overlap in the line of sight. A peculiar complication is that the variability of very close eclipsing binaries may not be solely due to the eclipses themselves, but also due to some intrinsic variability of the stars caused by the physical interactions they have with one another (Hilditch 2001). The dips in the light curves of a host star in an exoplanetary system is attributed to geometrical blocking of stellar light by a transiting planet, which gives crucial information for estimating the key physical parameter of the transiting planet (Mandel & Agol 2002).

With the recent increased availability of larger telescopes (e.g., $>$ 1 m) with a large field-of-view (FoV; e.g., $>$ one square degree field) for conducting time-series surveys, it has now become possible to systematically extend the study of variables to low amplitudes at the level of $\gtrsim$ milli-magnitudes and also to faint (e.g., B $>$ 21 magnitudes) objects. This can not only increase

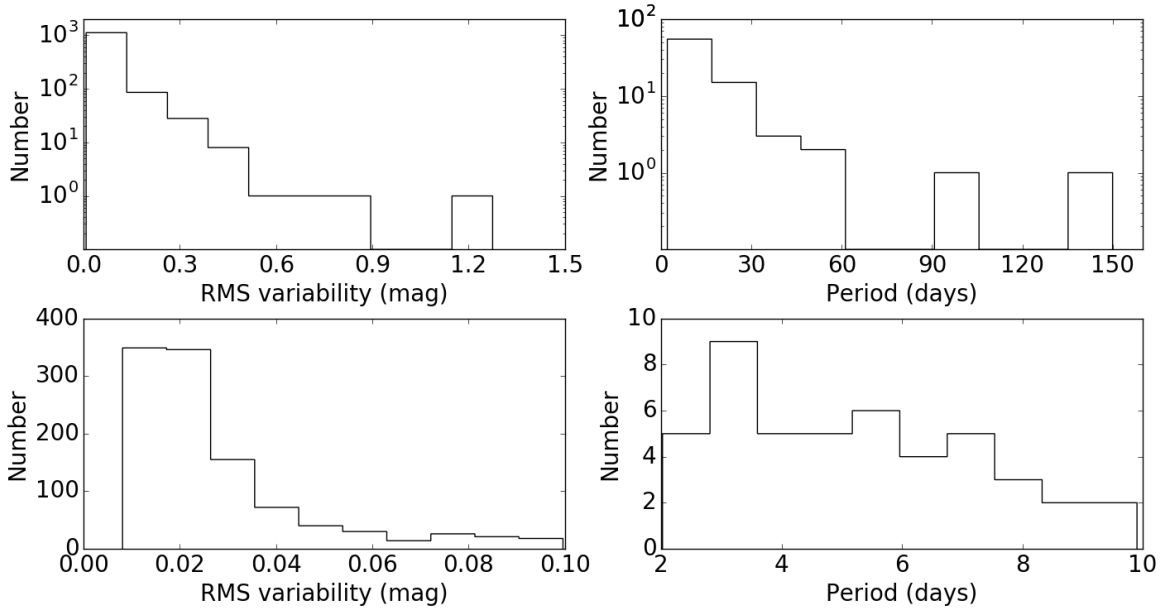

Figure 2. *Left:* Histograms of the RMS (root mean square) variability in B filter, for all the objects (top) and just the ones with low RMS variability < 0.1 magnitudes (bottom). *Right:* Histograms of the periods as given by the Fourier transforms, including all periods (top) and just low periods < 10 days (bottom). Note the logarithmic y-scale in the two top plots and the linear y-scale in the two bottom plots. For each of these histograms, we use 10 uniform bins.

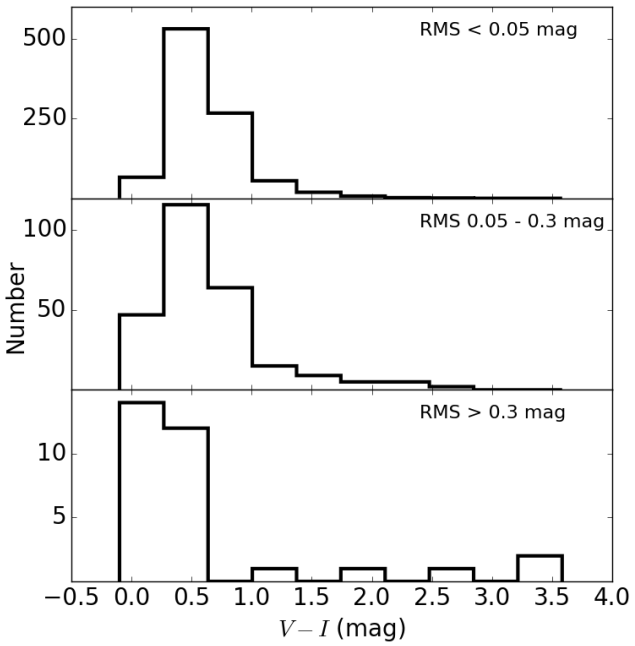

Figure 3. $V - I$ color histograms separated by RMS variability. We used 10 uniform bins for each of the histograms.

the sample size of previously-known types of variables, it can also discover previously unknown variables types and phenomena. These new surveys will shed new light to our understanding of variable objects and related astrophysics. Furthermore, as these surveys continuously monitor variable stars, we can measure changes in periods and instabilities (Turner et al. 2006; Smith 2013; Neilson et al. 2012; Neilson & Ignace 2014).

In this paper, we present our first results on variable objects from the KMTNet Supernova Program (KSP; Moon et al. 2016) from a 20 square degree field toward NGC 2784. KSP is a high-cadence (i.e., several exposures during a 24-h cycle), multi-color (BVI) search program of rapidly-evolving transients at early phases, focusing on discovery and monitoring of infant (i.e., less than a few hours from the explosion) supernovae using $\sim$ 17% of the entire observing time of the Korea Microlensing Telescope Network (KMTNet; Kim et al. 2016) in 2015–2019. The high-cadence, multi-color data from KSP using the network of three telescopes of 1.6-m size and $2^\circ \times 2^\circ$ FoV, located in Chile, South Africa, and Australia, provides an unprecedented serendipitous opportunity of extending the variable study to the regimes of small amplitudes and faint variables.

We organize our paper as follows: Section 2 includes the details about our observations and data reduction methods; Section 3 describes our analyses of the sources that we identify in their variability, color and period; Section 4 details our classifications of the variable sources, and Section 5 provides a summary of our results alongside our conclusions.

2. Observations and Data

Over $\sim$120 days between 2015 March and June during the KMTNet commissioning runs, KSP monitored five fields, totaling 20 square degrees, toward NGC 2784, (α, δ) = ($09^{\rm h}20^{\rm m}19.4^{\rm s}$, $-24^\circ10'20''$) (J2000), in search

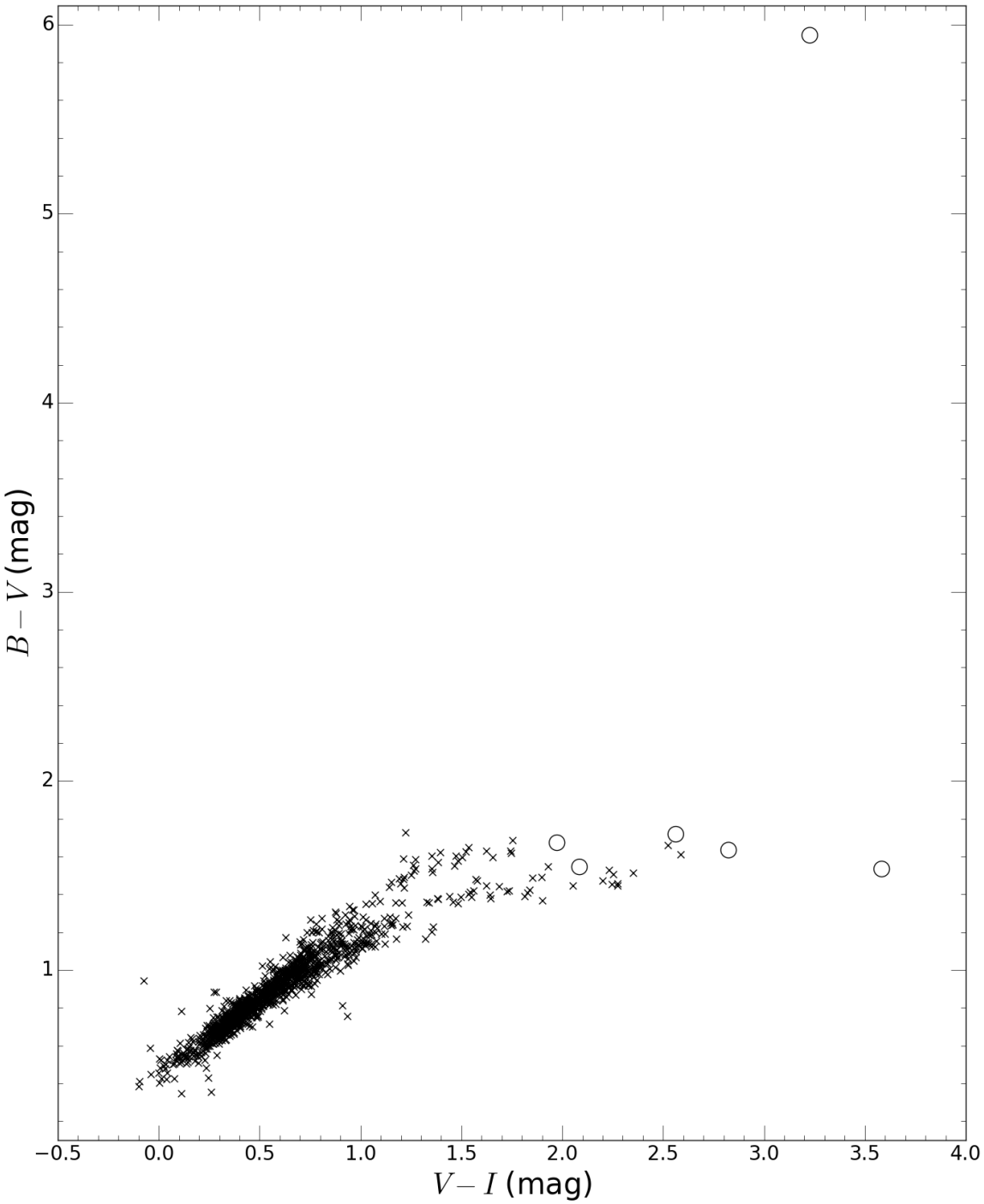

Figure 4. $B-V$ vs. $V-I$ color-color diagram showing all the stars in our sample. Circles indicate long period variables with periods greater than 50 days; crosses denote the rest of the population.

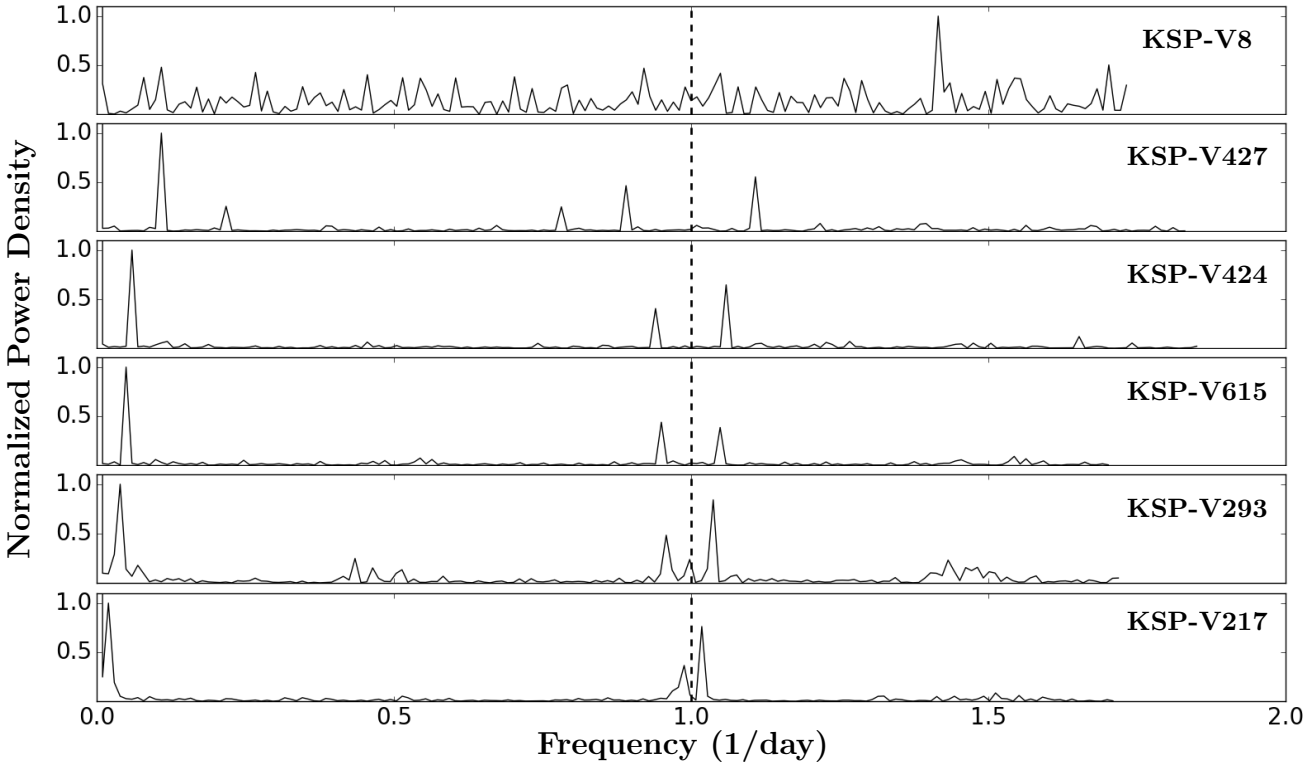

Figure 5. Sample of power spectra based in B filter for periodic objects, after re-binning data and re-normalizing the spectra to the peak amplitude. The dotted line highlights the 1 day^{-1} frequency. The periods identified are: (KSP-V8) 0.7, (KSP-V429) 9.2, (KSP-V426) 16.8, (KSP-V618) 20.2, (KSP-V294) 25.3, and (KSP-V217) 50.6 days.

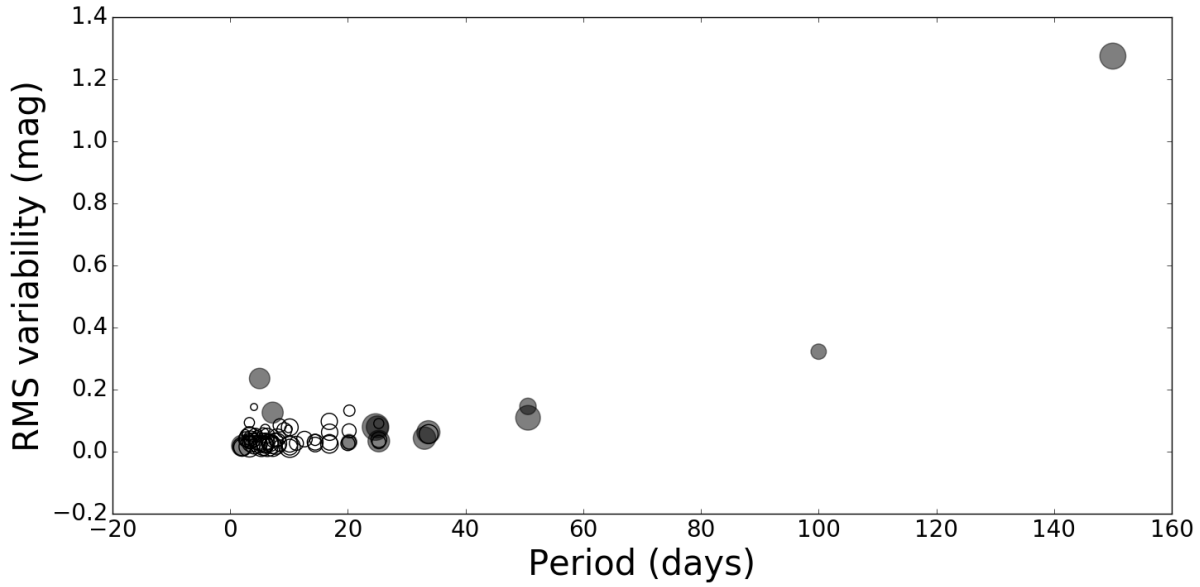

Figure 6. RMS variability vs. Period plot in the B filter. Marker size indicates relative median B magnitude (a larger marker means the object is brighter) while filled-in markers denote saturated objects (saturated in any filter).

of optical transients. The exact coordinates of the fields are available in Park et al. (2016). The NGC 2784 galaxy group was chosen because of its large sky coverage at the declination of $\sim$ –24.2° and a relatively nearby distance of $\sim$10 Mpc (e.g., Karachentsev et al. 2014), which makes it a good target for testing the performance of a new facility like the KMTNet with

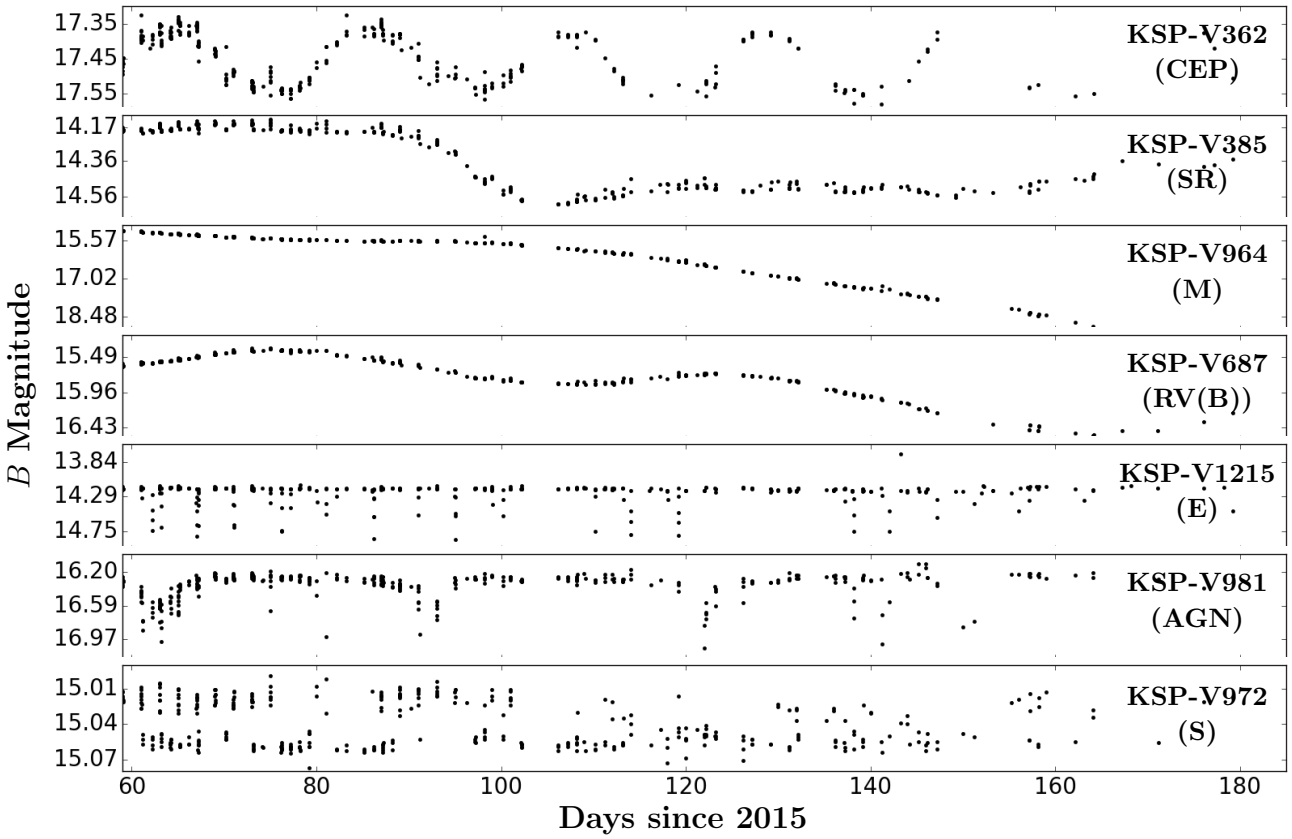

Figure 7. B filter light curves of a sample of objects for each classification type in Tables 1 & 2. We use the same acronyms defined in the caption of Figure 1 to represent the different variable types. From top to bottom, their details (classification, B band RMS variability, period) are listed as follows: KSP-V362 (CEP, 0.132 magnitudes, 20.3 days); KSP-V385 (SR, 0.173 magnitudes, unknown); KSP-V964 (M, 0.809 magnitudes, >150 days); KSP-V687 (RV(B), 0.261 magnitudes, unknown); KSP-V1215 (E, 0.135 magnitudes (depth of 0.552 magnitudes), unknown); KSP-V981 (AGN, 0.157 magnitudes, unknown); and KSP-V972 (S, 0.019 magnitudes, 2.0 days).

a long-monitoring observational campaign as reported here. Additionally, only a handful of low surface brightness dwarf galaxies have been identified from this group (Karachentsev et al. 2014), while the deep multi-color stacked images obtainable in KSP are ideally suited to finding more such objects. In fact, Park et al. (2016) recently identified more than 30 new dwarf galaxies in this group from the KSP data.

We obtained a total of 1379 images almost equally distributed among three different bands of BVI. The average cadences of the observations are 0.29, 0.26 and 0.25 days for B, V, and I, respectively. All images were obtained with 60-s exposure times in the BVI bands, which gave the typical limiting magnitudes of a point source in the images to be $\sim$ 21.5 magnitudes in all the BVI bands at S/N $\simeq$ 5. After flat fielding and the initial correction of CCD cross talks, an astrometic solution was then obtained for each image using the distortion map that we empirically derived for the KMTNet CCD images. We construct a reference image by stacking images taken only under 1.″2 seeing condition or better. From all the B band images, we then subtract the reference image in order to identify candidates of variable sources.

We base our variability analysis in the B filter because fewer objects are saturated in B than in V or I. The candidates are then confirmed to be real after careful investigation of their entire BVI light curves; as a result, we identify a total of 1247 variable point sources in our data.[1] (See Moon et al. (2016) for the details of the KSP data reduction and how reliable transient/variable sources are identified avoiding false alarms.) In addition, for each identified object, we filtered the data to exclude those with exceedingly high magnitude error ($>$ 3 standard deviations above the mean) in either the target or the reference star, and to include only those points which are within 0.″4 of the mode of the offset positions from the target position. We carried out differential photometric calibration of our variable sources using BVi magnitudes of isolated, nearby APASS standard stars from the AAVSO photometric all-sky survey[2]. The AAVSO survey uses the same BV filters as our program, and our analyses showed that our photometric solutions recovered the BV photometry of

[1] All our data for these identified variable objects will be available in the KMTNet project web page in the near future.
[2] https://www.aavso.org/apass

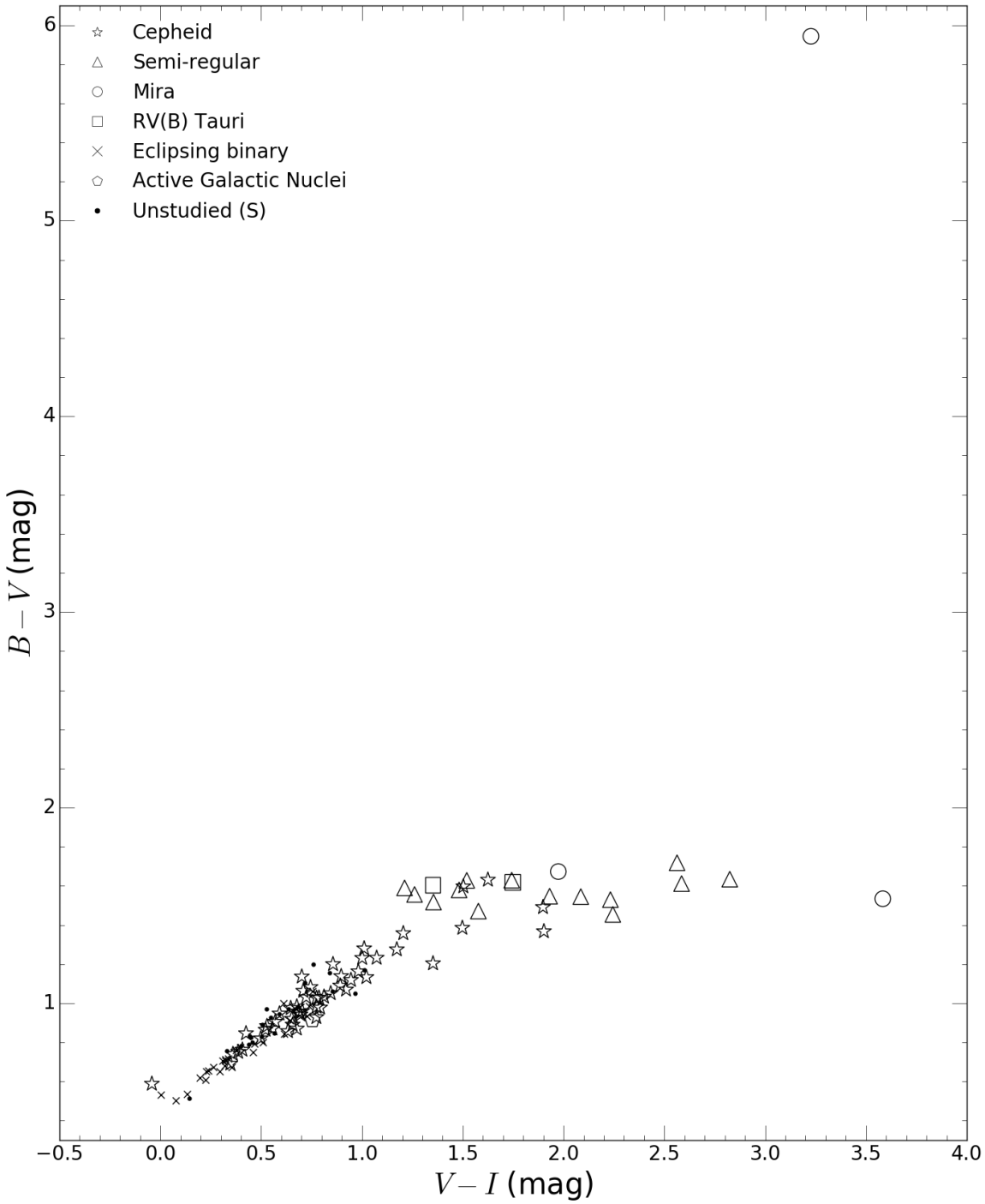

Figure 8. $B-V$ vs. $V-I$ color-color diagram showing all periodic and irregular objects in our sample (all objects in Tables 1 and 2, classified into their variable types. Three objects (KSP-V419, V729, and V757) are not plotted here as they were not detected in the I band.

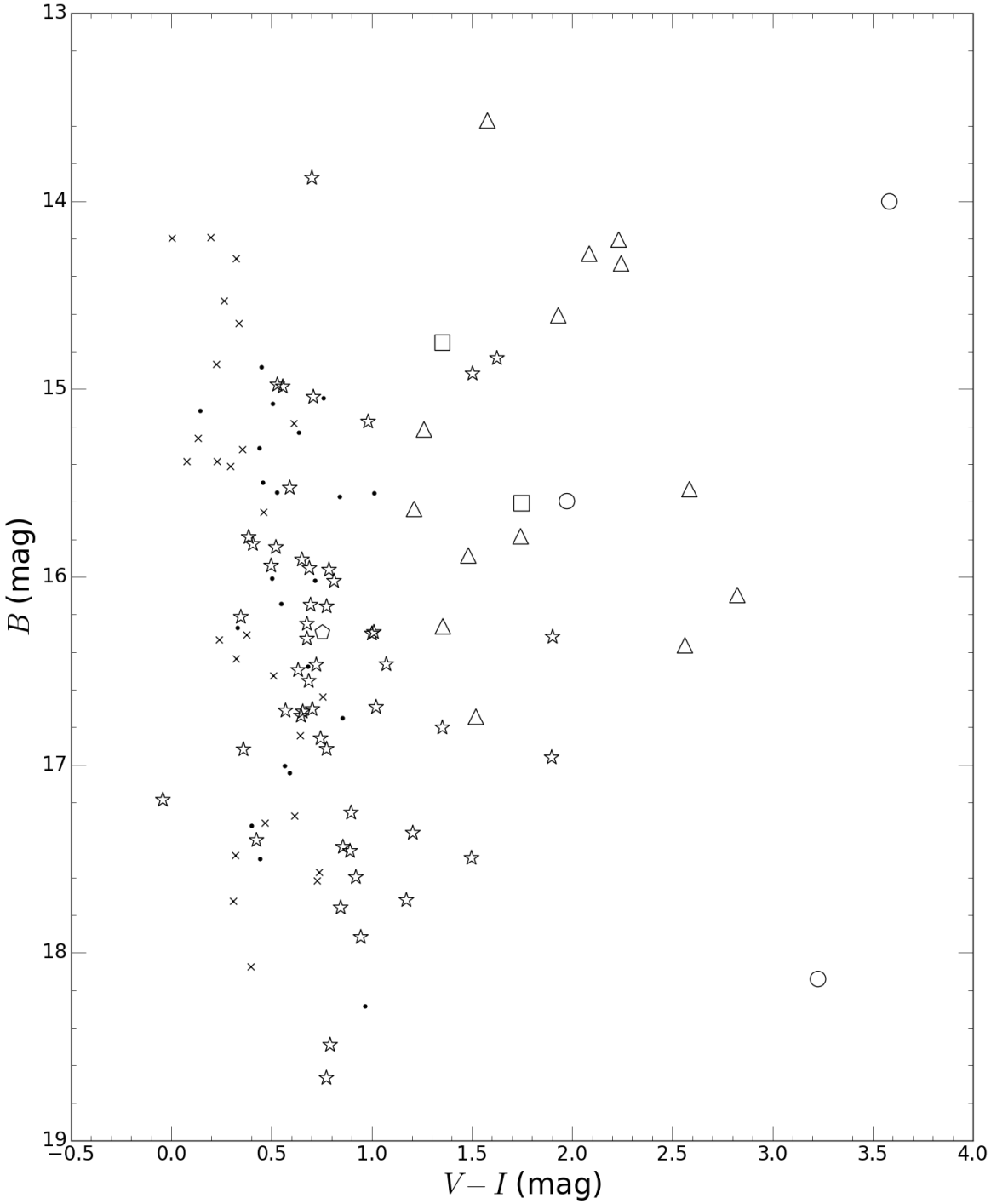

Figure 9. B vs. $V-I$ color-magnitude diagram showing all periodic and irregular objects in our sample (all objects in Tables 1 and 2, classified into their variable types. We use the same legend as in Figure 8. Three objects (KSP-V419, V729, and V757) are not plotted here as they were not detected in the I band.

AAVSO at the uncertainty level 0.02 magnitudes. We used the i band photometry of the AAVSO survey to obtain the I band photometric solution of our variable sources which recovered i band photometry at the level of 0.04 magnitudes. We believe the small difference in the filter transmission between the i and I bands are responsible for the increased uncertainty in the I band photometric solution. All the standard stars that we used have magnitudes in the range of 15.0–17.0 (B), 14.5–15.7 (V) and 13.0–15.5 (i) magnitudes, and the typical uncertainty of the magnitudes is $\sim$0.01 magnitudes. Their brightness stayed constant in all the images obtained by KSP. Figure 1 shows B-band light curves of a sample of 10 variable sources that we identify with noticeably different periods (see below).

3. Variability, Color and Period

We use the B-band root mean square (RMS) magnitudes of the variable sources to characterize their overall variability, which has the advantage of not relying on maximum and minimum magnitudes which may be missed by our observations. Figure 2 (plots in the left hand side) show the histogram of their RMS values. The RMS values of the B-band magnitudes range between 0.008 and 1.275 magnitudes, while the majority, 1123, belong to the first bin of < 0.135 magnitudes (the top-left plot in Figure 2). The number of variable sources declines rapidly as the RMS increases.

Figure 3 shows $V - I$ color histograms of the variable sources. We divide the sources into three groups based on the magnitude of their variability: (1) high-variability group of 31 sources that have B-band RMS greater than 0.3 magnitudes; (2) medium-variability group of 265 sources with B-band RMS between 0.05 and 0.3 magnitudes; (3) low-variability group of the remaining sources smaller than 0.05 magnitudes. Four sources in the high-variability group have periods longer than 100 days (see below for period determination). They are very red with $V - I \gtrsim 2.0$ magnitudes and all of them are saturated at least in one of the BVI bands. We determine the periods of 26 sources in the medium-variability group between 2 and 51 days, whereas 49 sources in the low-variability group have periods in the range of 2–33 days.

While all the three groups have their histogram peak around $V - I \simeq 0.5$ magnitudes, the relative number of sources redder than $V - I \gtrsim 1.0$ magnitudes to the total number of sources in each group is much larger in the high-variability group. The high-variability group, therefore, is populated with an increased number of redder sources. Four of the six long-term variable sources in Figure 4 belong to the high-variability group, while the other two belong to the medium-variability group.

We present a color-color diagram in Figure 4 which compares $B-V$ and $V-I$ colors of the variable sources. We use the median magnitudes in each band for color calculation. There is a good correlation between the two colors at $V - I < 1.5$ magnitudes after which the correlation breaks off with $B - V$ flattened due to saturation. This indicates that the saturation effect becomes more significant in the V and I bands than B, consistent with the interpretation that the brighter sources are more likely to be late types such as giants or supergiants. All the variable sources with periods longer than 50 days (i.e., open circles in Figure 4) are at the redder end of the $V - I$ color distribution and are all saturated. This again supports the interpretation that long-term variables are giants or supergiants.

We determine periods of the variable sources showing clear periodicity mainly using Fourier transformation techniques and power-density analyses. (Note that for sources whose period is longer than 60 days, we rely on visual inspection because our observing duration is $\sim$120 days.) In order to apply the Fourier transformation to our time series we first re-binned the B-band data to an evenly spaced time domain, with time spacing equal to the average cadence. The average time spacing for each source is 0.30 ± 0.05 days. When there is a significant gap in the data, we used the median values of the light curves. Given the sampling rate of $\sim$0.30 days, we only consider the periods longer than 2 days reliable and exclude those shorter than 2 days in the analyses. As a result, we have 77 sources in total with reliable period determination. In the histogram plots of the periods in Figure 2 (right-hand panels), 55 sources out of 77 are in the first bin with periods shorter than 16.8 days, and the number of sources sharply decreases as period increases. The longest estimated period is $\sim$150 days, which we determine by visual inspection, while two sources appear to have periods longer than 150 days (see Figures 1 & 7). (Note that the latter two sources are excluded from the histograms in Figure 2.)

Figure 5 shows power-density spectra of six sources whose light curves are presented in Figure 1: one rapidly variable source (KSP-V8) and five periodic sources (KSP-V429, V426, V618, V294 and V217). As expected, while the first source does not have any clear power-density peak, the five other sources show prominent low-frequency (< 0.5 day^{-1}) peaks. There exist in the figure additional secondary peaks which are symmetrically placed around the frequency of 1 day^{-1}. Their displacements from the 1 day^{-1} frequency are equal to the frequencies of their peaks. These sidelobes are caused by the frequency modulations between two periodic signatures from the source and 1-day observing cycle (or earth rotation). Similar behaviours in the power-density spectra caused by frequency modulations between two periodic signals have previously been observed (see Moon & Eikenberry 2001a,b, for examples).

Figure 6 compares the periods of the variable sources with their B-band RMS variability, where we can identify the correlation between the two parameters for long-period, i.e., ≥ 20 days variables. This is because the long-period variables change their brightness more significantly than the short-period counterparts. We note that most of the long-period variables are saturated, indicating that they are mostly from giants or supergiants than main sequence stars.

Table 1
Table of periodic (> 2 days) and semi-periodic objects in our sample.

Object id.	R.A. (J2000) [H:M:S]	Dec. (J2000) [D:M:S]	B [mag]	V [mag]	I [mag]	$B-V$	$V-I$	B RMS [mag]	Period [days]	Type
KSP-V0	09:09:14.999	-22:25:06.2	15.17	14.01	13.03	1.16	0.98	0.236	5.0	CEP
KSP-V4	09:09:28.654	-22:13:05.4	14.00	12.47	8.88	1.53	3.58	1.275	∼150	M
KSP-V20	09:10:59.741	-22:15:55.1	15.95	15.00	14.31	0.95	0.69	0.021	7.2	CEP
KSP-V21	09:12:03.836	-21:39:04.6	13.88	12.74	12.04	1.14	0.70	0.079	24.7	CEP
KSP-V26	09:12:16.014	-22:19:18.8	17.50	16.11	14.61	1.38	1.50	0.038	14.4	CEP
KSP-V71	09:04:51.235	-22:21:38.6	16.29	15.01	14.00	1.28	1.01	0.039	25.3	CEP
KSP-V75	09:07:44.822	-22:21:30.1	14.84	13.21	11.58	1.63	1.62	0.080	25.0	CEP
KSP-V77	09:07:13.673	-22:32:12.9	16.25	15.27	14.59	0.98	0.68	0.031	14.4	CEP
KSP-V80	09:05:46.606	-21:48:12.6	14.88	14.06	13.61	0.83	0.45	0.020	6.3	S
KSP-V84	09:08:20.856	-22:34:18.1	14.75	13.15	11.80	1.61	1.35	0.044	33.0	RV(B)
KSP-V85	09:07:35.937	-22:17:39.9	18.28	17.23	16.27	1.05	0.97	0.058	2.6	S
KSP-V88	09:05:28.737	-22:00:09.6	15.31	14.52	14.08	0.79	0.44	0.020	5.6	S
KSP-V90	09:07:02.893	-22:32:24.1	15.57	14.42	13.58	1.16	0.84	0.016	2.0	S
KSP-V115	09:08:21.588	-21:47:32.2	18.49	17.51	16.72	0.98	0.79	0.073	9.9	CEP
KSP-V118	09:10:38.695	-23:22:28.7	16.36	14.65	12.08	1.72	2.56	0.322	∼100	SR
KSP-V126	09:08:42.340	-23:10:18.4	14.92	13.32	11.82	1.60	1.50	0.034	25.3	CEP
KSP-V128	09:09:09.717	-22:46:23.8	16.75	15.69	14.84	1.06	0.85	0.053	4.3	S
KSP-V131	09:09:44.572	-23:37:48.9	15.55	14.38	13.37	1.17	1.01	0.030	6.0	S
KSP-V132	09:10:19.854	-23:28:44.5	14.61	13.06	11.13	1.55	1.93	0.063	33.7	SR
KSP-V136	09:11:05.938	-22:49:07.6	15.50	14.70	14.24	0.80	0.46	0.029	3.6	S
KSP-V168	09:05:50.509	-22:57:30.9	15.96	14.93	14.15	1.03	0.79	0.028	6.8	CEP
KSP-V182	09:04:33.827	-23:18:27.0	15.55	14.58	14.05	0.97	0.53	0.015	7.2	S
KSP-V187	09:05:56.312	-23:13:36.5	16.30	15.07	14.07	1.23	1.00	0.030	16.9	CEP
KSP-V199	09:07:21.667	-23:06:04.9	17.19	16.60	16.64	0.59	-0.04	0.034	7.2	CEP
KSP-V209	09:05:28.441	-23:21:49.4	17.36	16.00	14.80	1.36	1.20	0.024	6.3	CEP
KSP-V210	09:08:16.065	-23:43:35.5	17.04	16.10	15.51	0.94	0.59	0.032	3.5	S
KSP-V217	09:12:06.342	-24:12:29.2	16.10	14.46	11.64	1.63	2.82	0.146	50.6	SR
KSP-V223	09:13:31.802	-23:23:31.4	18.14	12.20	8.97	5.94	3.23	0.372	>150	M
KSP-V293	09:12:10.842	-23:59:08.6	16.86	15.78	15.03	1.08	0.74	0.031	25.3	CEP
KSP-V304	09:13:28.630	-23:23:59.9	15.64	14.05	12.84	1.59	1.21	0.039	-	SR
KSP-V352	09:09:20.383	-24:23:21.0	15.23	14.26	13.62	0.97	0.64	0.017	5.3	S
KSP-V354	09:07:52.654	-24:15:17.8	17.72	16.45	15.27	1.27	1.17	0.094	3.3	CEP
KSP-V359	09:07:09.643	-23:57:18.2	16.48	15.49	14.81	0.98	0.68	0.040	2.7	S
KSP-V362	09:06:30.867	-24:05:01.9	17.44	16.24	15.38	1.20	0.86	0.132	20.3	CEP
KSP-V372	09:09:13.174	-24:18:25.4	16.14	15.22	14.67	0.93	0.55	0.017	-	S
KSP-V385	09:09:28.812	-23:58:54.9	14.21	12.68	10.44	1.53	2.23	0.173	-	SR
KSP-V397	09:06:27.791	-23:50:41.2	15.08	14.19	13.68	0.89	0.51	0.015	10.1	S
KSP-V419	09:11:27.426	-24:43:04.7	14.68	13.13	-	1.55	-	0.089	-	SR
KSP-V422	09:11:15.022	-25:15:30.0	15.78	14.15	12.41	1.63	1.74	0.095	-	SR
KSP-V424	09:11:09.673	-24:32:23.6	16.16	15.13	14.36	1.03	0.78	0.097	16.8	CEP
KSP-V427	09:14:11.453	-24:48:50.3	16.46	15.23	14.16	1.23	1.07	0.069	9.2	CEP
KSP-V435	09:14:06.804	-25:06:22.7	17.01	16.16	15.59	0.85	0.56	0.033	3.2	S
KSP-V449	09:10:21.253	-25:07:51.2	14.98	14.09	13.56	0.88	0.53	0.026	7.8	CEP
KSP-V475	09:13:45.747	-24:57:36.8	17.92	16.80	15.85	1.12	0.95	0.073	6.0	CEP
KSP-V497	09:06:10.222	-25:25:30.1	15.84	14.98	14.46	0.86	0.52	0.024	16.9	CEP
KSP-V509	09:05:23.909	-24:42:24.6	17.46	16.37	15.48	1.09	0.89	0.059	5.6	CEP
KSP-V510	09:08:26.076	-24:47:32.8	17.60	16.53	15.61	1.07	0.92	0.051	4.6	CEP
KSP-V542	09:06:50.897	-25:19:32.4	15.79	15.04	14.65	0.75	0.39	0.021	4.1	CEP
KSP-V612	09:16:53.084	-22:23:45.5	16.33	15.46	14.78	0.87	0.68	0.040	12.6	CEP
KSP-V615	09:18:56.197	-22:33:42.4	16.72	15.83	15.17	0.89	0.66	0.067	20.2	CEP
KSP-V627	09:16:41.836	-22:00:47.6	18.67	17.74	16.96	0.93	0.77	0.144	4.1	CEP
KSP-V630	09:19:18.257	-22:34:45.0	16.32	14.95	13.05	1.37	1.90	0.031	20.2	CEP
KSP-V687	09:15:10.263	-21:46:05.6	15.60	13.98	12.24	1.62	1.75	0.261	-	RV(B)
KSP-V692	09:12:47.247	-22:04:12.2	15.21	13.66	12.40	1.56	1.26	0.028	-	SR
KSP-V700	09:12:18.654	-21:49:15.9	16.74	15.12	13.60	1.63	1.52	0.050	-	SR
KSP-V705	09:16:19.356	-22:04:30.7	16.92	16.18	15.82	0.74	0.36	0.025	5.1	CEP
KSP-V723	09:13:28.346	-21:44:18.2	16.01	15.18	14.68	0.83	0.50	0.033	4.6	S
KSP-V729	09:12:41.492	-21:50:24.3	14.36	12.80	-	1.56	-	0.036	-	SR
KSP-V736	09:14:37.399	-22:31:28.0	16.55	15.60	14.91	0.96	0.69	0.023	14.4	CEP

Table 1
Continued

Object id.	R.A. (J2000) [H:M:S]	Dec. (J2000) [D:M:S]	B [mag]	V [mag]	I [mag]	$B-V$	$V-I$	B RMS [mag]	Period [days]	Type
KSP-V756	09:19:49.680	-23:39:03.9	15.91	14.99	14.34	0.92	0.65	0.045	8.0	CEP
KSP-V757	09:17:26.182	-22:48:12.1	15.07	13.45	-	1.62	-	0.193	-	SR
KSP-V759	09:19:38.059	-23:12:46.7	16.92	15.93	15.16	0.98	0.77	0.085	8.4	CEP
KSP-V760	09:20:31.284	-23:29:17.3	17.76	16.71	15.86	1.05	0.84	0.091	25.3	CEP
KSP-V761	09:18:09.084	-23:09:21.2	16.70	15.74	15.04	0.96	0.70	0.036	7.8	CEP
KSP-V777	09:19:44.347	-23:31:22.2	14.28	12.73	10.65	1.54	2.09	0.109	50.6	SR
KSP-V791	09:19:55.747	-23:40:20.7	14.33	12.88	10.63	1.45	2.24	0.045	-	SR
KSP-V797	09:17:40.654	-23:08:17.6	16.71	15.81	15.24	0.90	0.57	0.026	20.0	CEP
KSP-V799	09:19:55.533	-23:28:55.9	16.26	14.75	13.39	1.52	1.36	0.028	-	SR
KSP-V862	09:14:37.676	-23:24:48.8	16.27	15.51	15.19	0.76	0.33	0.015	10.1	S
KSP-V864	09:12:34.723	-22:51:01.2	17.25	16.12	15.22	1.14	0.90	0.033	4.1	CEP
KSP-V876	09:13:26.177	-23:12:11.1	17.50	16.67	16.22	0.83	0.44	0.040	3.2	S
KSP-V889	09:19:41.586	-24:18:37.3	15.53	13.92	11.34	1.61	2.59	0.168	-	SR
KSP-V890	09:20:59.546	-24:16:40.6	15.53	14.58	13.99	0.95	0.59	0.057	33.7	CEP
KSP-V904	09:18:21.460	-24:10:17.8	15.82	15.06	14.66	0.76	0.41	0.025	4.8	CEP
KSP-V947	09:19:11.071	-24:14:37.0	17.40	16.55	16.13	0.85	0.43	0.026	6.3	CEP
KSP-V951	09:21:16.474	-23:27:52.3	13.57	12.10	10.52	1.47	1.58	0.102	-	SR
KSP-V964	09:16:05.451	-23:39:19.4	15.60	13.92	11.95	1.67	1.97	0.809	>150	M
KSP-V972	09:16:36.563	-24:07:11.6	15.05	13.85	13.09	1.20	0.76	0.019	2.0	S
KSP-V980	09:16:32.537	-24:07:59.2	16.02	14.91	14.19	1.11	0.72	0.014	2.0	S
KSP-V1025	09:19:53.740	-24:33:30.2	16.47	15.44	14.71	1.03	0.72	0.051	6.3	CEP
KSP-V1027	09:18:14.192	-25:13:46.2	14.99	14.12	13.56	0.87	0.56	0.044	3.4	CEP
KSP-V1029	09:20:14.042	-25:05:10.6	15.89	14.31	12.82	1.58	1.48	0.041	-	SR
KSP-V1035	09:18:12.098	-25:01:09.5	15.94	15.12	14.62	0.82	0.50	0.023	6.0	CEP
KSP-V1045	09:20:30.398	-25:24:08.6	16.69	15.56	14.54	1.13	1.02	0.027	11.2	CEP
KSP-V1059	09:14:38.158	-24:43:36.7	15.04	13.98	13.27	1.06	0.71	0.126	7.2	CEP
KSP-V1065	09:15:46.492	-25:22:40.3	16.15	15.21	14.51	0.94	0.70	0.063	16.9	CEP
KSP-V1091	09:16:14.023	-24:38:07.8	17.32	16.54	16.14	0.78	0.40	0.019	8.4	S
KSP-V1107	09:25:12.799	-21:53:56.1	16.80	15.60	14.25	1.20	1.35	0.058	3.3	CEP
KSP-V1108	09:24:43.543	-22:17:21.5	16.50	15.64	15.01	0.86	0.63	0.043	3.5	CEP
KSP-V1156	09:27:00.105	-22:03:08.3	15.12	14.60	14.46	0.51	0.14	0.016	3.3	S
KSP-V1163	09:21:16.693	-22:14:18.2	16.02	14.99	14.18	1.03	0.81	0.078	10.1	CEP
KSP-V1178	09:22:32.921	-21:58:22.7	16.96	15.47	13.57	1.49	1.90	0.031	3.5	CEP
KSP-V1211	09:24:51.976	-23:12:29.5	16.21	15.52	15.18	0.69	0.35	0.024	10.1	CEP
KSP-V1214	09:28:26.615	-23:22:16.1	16.74	15.76	15.12	0.98	0.65	0.031	20.2	CEP

Column (1) lists the id. names of our objects. Columns (2) and (3) list the right ascension (R.A.) and declination (Dec.) respectively, columns (4), (5), and (6) list the median magnitudes in the B, V, and I filters respectively, columns (7) and (8) contain the $B-V$ and $V-I$ colors respectively, calculated from the median magnitudes, column (9) denotes the RMS variability in the B filter, and column (10) contains the periods as given by their B filter Fourier spectrum (values denoted with $\sim$ or $>$ indicate periods estimated by eye; non-values (-) indicate irregular/semi-periodic objects). We use the same acronyms defined in the caption of Figure 1 to represent the different variable types, as listed in column (11).

4. Classifications and Variable Types

Out of 1247 variable sources, we are able to classify 121 sources in a reliable manner to be candidates of known variable types and active galactic nuclei (AGN) largely based on the criteria from Samus et al. (2009) as explained below. In conclusion, we classify 121 sources as these candidates: (1) Cepheids (CEP), 51 sources; (2) semi-regular (SR) variables, 17 sources; (3) Mira variables (M), 3 sources; (4) RV(B) Tauri variables, 2 sources; (5) eclipsing binaries (E), 26 sources; (6) AGN, 1 source; and (7) unstudied variables of rapid variability (S), 21 sources. Sample light curves of candidates for these different types of variables are shown in Figure 7. Tables 1 and 2 contain parameters of these 121 variable sources that we classify: the former is for the 94 candidates for the types other than eclipsing binary or AGN, including the 77 sources with reliable period determination (Section 3); the latter is for the 27 candidates for eclipsing binary or AGN. We use the SIMBAD database to confirm 14 sources from Table 1 and 4 sources from Table 2 as previously known variable objects or AGN. These 14 sources from Table 1 include the three Mira types (KSP-V4, V223, V964) and one SR variable (KSP-V757), as we classify (Christiansen et al. 2008), whereas the remaining 10 sources have either no classification (KSP-V385, V419, V729, V791, V951; Siebert et al. 2011; Cutri et al. 2003; Zacharias et al. 2003) or are classified as just long period variables (KSP-V21, V118, V132, V687, V889; Christiansen et al. 2008). Two of these 14 previously-known sources have known periods, KSP-V757 with a 59 day period and KSP-V889 with a 36 day period (Christiansen et al.

Table 2
Table of eclipsing binary candidates and AGN (last row) in our sample.

Object id.	R.A. (J2000) [H:M:S]	Dec. (J2000) [D:M:S]	B [mag]	V [mag]	I [mag]	$B-V$	$V-I$	B RMS [mag]	B Depth [mag]
KSP-V2	09:10:31.816	-21:58:06.8	15.41	14.76	14.47	0.65	0.29	0.163	0.533
KSP-V16	09:11:06.649	-22:30:13.5	17.31	16.52	16.05	0.79	0.47	0.116	0.549
KSP-V162	09:05:12.719	-23:20:12.2	15.18	14.18	13.57	1.00	0.61	0.108	0.437
KSP-V219	09:13:22.691	-24:18:23.7	16.31	15.55	15.17	0.76	0.38	0.128	0.420
KSP-V227	09:12:03.514	-24:17:35.9	17.57	16.59	15.85	0.99	0.74	0.130	0.473
KSP-V344	09:07:09.421	-23:54:34.4	16.64	15.58	14.82	1.06	0.76	0.208	0.903
KSP-V512	09:06:50.493	-24:45:09.6	17.62	16.68	15.96	0.94	0.73	0.144	0.559
KSP-V531	09:05:30.908	-25:02:52.3	14.53	13.86	13.59	0.67	0.26	0.090	0.388
KSP-V556	09:05:26.030	-24:51:49.9	16.43	15.73	15.41	0.71	0.32	0.109	0.570
KSP-V724	09:15:48.485	-21:41:48.2	16.84	15.93	15.29	0.91	0.64	0.196	1.080
KSP-V754	09:18:04.322	-23:00:44.9	14.65	13.93	13.60	0.72	0.33	0.097	0.350
KSP-V755	09:19:07.585	-23:43:47.4	15.39	14.88	14.81	0.50	0.08	0.082	0.269
KSP-V836	09:20:20.164	-23:27:54.3	15.26	14.72	14.59	0.54	0.13	0.040	0.130
KSP-V866	09:14:12.674	-22:57:29.3	17.73	17.02	16.71	0.71	0.31	0.076	0.333
KSP-V871	09:15:49.367	-23:15:08.3	15.39	14.73	14.51	0.65	0.23	0.057	0.460
KSP-V892	09:19:57.588	-24:01:36.3	16.33	15.68	15.44	0.65	0.24	0.119	0.454
KSP-V977	09:14:52.620	-24:14:56.0	14.20	13.67	13.66	0.53	0.00	0.170	0.616
KSP-V1040	09:20:37.067	-24:44:50.1	18.07	17.30	16.90	0.78	0.39	0.128	0.478
KSP-V1068	09:14:40.542	-24:46:06.7	17.48	16.80	16.48	0.68	0.32	0.198	0.684
KSP-V1099	09:25:23.743	-22:10:15.6	14.87	14.26	14.04	0.61	0.22	0.211	0.747
KSP-V1106	09:26:29.337	-22:12:20.4	16.52	15.72	15.21	0.80	0.51	0.119	0.513
KSP-V1158	09:25:00.586	-22:01:05.4	14.30	13.59	13.27	0.71	0.32	0.052	0.255
KSP-V1171	09:21:30.857	-22:06:08.1	15.32	14.65	14.29	0.68	0.36	0.101	0.571
KSP-V1197	09:20:18.195	-21:51:10.5	17.27	16.43	15.81	0.84	0.62	0.056	0.183
KSP-V1208	09:27:08.355	-23:06:41.9	15.65	14.90	14.44	0.75	0.46	0.054	0.227
KSP-V1215	09:28:14.859	-22:57:54.8	14.19	13.57	13.38	0.62	0.20	0.135	0.552
KSP-V981	09:16:46.734	-24:20:41.7	16.30	15.38	14.63	0.91	0.75	0.157	(AGN)

Column (1) lists the id. names of our objects. Columns (2) and (3) list the right ascension (R.A.) and declination (Dec.) respectively, columns (4), (5), and (6) list the median magnitudes in the B, V, and I filters respectively, columns (7) and (8) contain the $B-V$ and $V-I$ colors respectively, calculated from the median magnitudes, column (9) denotes the RMS variability in the B filter, and column (10) includes the estimated depths of the eclipses in the B filter.

2008), although we were unable to calculate the periods of these objects. Among the four previously-known sources from Table 2, three (KSP-V871, V977, V1099) are classified as eclipsing binaries (Christiansen et al. 2008; Malkov et al. 2006) while the other one (KSP-V981) is an AGN (Jones et al. 2009). This shows that our classification is overall in a good agreement with previous results. Table 3 gives the names of the 18 previously known objects as given on SIMBAD.

All the variables with a clear period between 2 and 135 days have B-band RMS variability in the range of 0.021–0.236 magnitudes with the average of 0.054 magnitudes. Their magnitude difference between the maximum and minimum changes in the range of 0.100–0.825 magnitudes. This period range and magnitude difference make them proper candidates for Cepheid variables according to Samus et al. (2009). Our classification of candidates for Cepheids is indistinguishable between Type I and Type II. Additional careful analysis is required to further classify them into Cepheid subtypes. They mostly belong to the low- or medium-variability group, and their average period is 11.9 ± 7.8 days – the minimum and maximum are 3.3 and 33.7 days, respectively.

The SR variable candidates are those with smoothly-varying light curves but without any definitive periodicity, sometimes showing evolving periods or even durations of constant magnitude. According to Samus et al. (2009), SR variables have quite irregular periodicity which ranges from as small as 20 days to greater than 2000 days. This makes it very difficult for us to estimate any reliable periods for our SR variable candidates due to their intrinsic irregularity and periods longer than the duration of our observations. Our close inspection of their light curves show that while a few of them likely have periods shorter than 50 days, a significant portion of them seem to have patterns lasting much longer. The B-band RMS variability of the SR candidates is between 0.028 and 0.322 magnitudes.

The three candidates of the Mira-type variables have already been identified as such (Samus et al. 2003, 2009), confirming our classification. The B-band RMS variabilities of the three variables are 0.372, 0.809 and 1.275 magnitudes, respectively, and their periods are $\gtrsim$ 150 days. They have the largest RMS variability as well as longest periods, with very red colors.

We classify two peculiar variable sources to be candidates for RV(B) Tauri variables primarily because their light curves show complex periodicity with potentially more than one period. In other words, while

Table 3
Table matching the previously known objects in our sample to their references.

Object id. in this paper	Name in SIMBAD	Reference
KSP-V4	V* CC Pyx	Samus et al. (2009)
KSP-V21	2MASS J09120383-2139049	Christiansen et al. (2008)
KSP-V118	2MASS J09103869-2322291	Christiansen et al. (2008)
KSP-V132	2MASS J09101984-2328449	Christiansen et al. (2008)
KSP-V223	V* IQ Hya	Samus et al. (2009)
KSP-V385	2MASS J09092880-2358551	Siebert et al. (2011)
KSP-V419	2MASS J09112745-2443054	Cutri et al. (2003)
KSP-V687	2MASS J09151029-2146054	Christiansen et al. (2008)
KSP-V729	UCAC2 23120346	Zacharias et al. (2003)
KSP-V757	V* V384 Hya	Christiansen et al. (2008)
KSP-V791	UCAC2 22220153	Zacharias et al. (2003)
KSP-V871	2MASS J09154938-2315085	Christiansen et al. (2008)
KSP-V889	2MASS J09194157-2418373	Christiansen et al. (2008)
KSP-V951	2MASS J09211650-2327522	Siebert et al. (2011)
KSP-V964	V* V521 Hya	Samus et al. (2009)
KSP-V977	2MASS J09145262-2414562	Christiansen et al. (2008)
KSP-V981	2MASX J09164671-2420414	Jones et al. (2009)
KSP-V1099	V* XZ Hya	Malkov et al. (2006)

This list includes 18 objects in total, with 14 from Table 1 and 4 from Table 2; their object id. in this paper is listed in column (1), their name as appearing on SIMBAD is shown in column (2), and their primary reference is listed in column (3).

Table 4
Summary of our variable candidates grouped into their classified types.

Type	Number of candidates	B RMS (mean) [mag]	$B-V$ (mean) [mag]	$V-I$ (mean) [mag]	Periods [days]
CEP	51	0.021-0.236 (0.054)	0.59-1.63 (1.04)	−0.04-1.90 (0.82)	3.3-33.7
SR	17	0.028-0.322 (0.102)	1.45-1.72 (1.57)	1.21-2.82 (1.90)	∼100-unknown
M	3	0.372-1.275 (0.819)	1.53-5.94 (3.05)	1.97-3.58 (2.83)	∼150-unknown
RV(B)	2	0.044-0.261 (0.153)	1.61-1.62 (1.61)	1.35-1.75 (1.55)	33.0-unknown
E	26	0.040-0.211 (0.119)	0.50-1.06 (0.74)	0.00-0.76 (0.38)	unknown
AGN	1	0.157	0.91	0.75	-
S	21	0.014-0.058 (0.026)	0.51-1.20 (0.92)	0.14-1.01 (0.59)	4.5-10.1, unknown

We use the acronyms defined in the caption of Figure 1 to represent the different variable types in column (1). Column (2) lists the number of candidates identified. Columns (3) through (5) show the ranges of B RMS variability, $B-V$ color, and $V-I$ color, respectively, with the mean in parentheses. Column (6) lists the range of periods if known or applicable.

their light curves show that their brightnesses change with a period longer than 120 days, which is our measurement limit for periods, there exists a clear pattern of shorter term variability. These peculiar behaviors belong to those of RV(B) Tauri variables (Samus et al. 2009). The B-band RMS variabilities of the two candidates are 0.044 and 0.261 magnitudes, respectively.

The 26 candidates for eclipsing binaries are a collection of sources exhibiting constant brightness with clear recurrent sharp dips, which is characteristic of binary stars in eclipsing configuration (Percy 2007). Their B-band RMS variability is in the range of 0.040–0.211 magnitudes and the average is 0.120 magnitudes. We do not have reliable period measurements of these candidates. The coordinate of the one AGN source overlaps with the previously known coordinate of the AGN 2MASX J09164671-2420414 (Jones et al. 2009) which appears as an extended source in our images. Therefore, we believe the variability that we detected from this source is not from a variable star but from the AGN variability (Jones et al. 2009).

Following Samus et al. (2009), we classify the rest of the variable sources in Table 1 to be candidates for 'unstudied variable stars with rapid changes.' (Note that these variables are denoted by the character 'S' in Samus et al. 2009.) These are variable sources that do not belong to the aforementioned types and they do not show reliable periodicities in our light curves. There are 21 such sources in our sample, with the B-band RMS variability of 0.026 ± 0.013 magnitudes.

Figure 8 shows a ($B-V$ vs. $V-I$) color-color diagram of the variable sources denoting their types with different symbols. The 51 Cepheid candidates have a wide range of colors and appear to be independent of them with all members showing $V-I$ color smaller than 2 magnitudes. The SR candidates and Mira variables are very red: the $V-I$ colors of the former vary between 1.21 and 3.58 magnitudes; the latter are > 1.97 magnitudes. This agrees well with their classification because both the types are known to be giants or supergiants of late type stars (Samus et al. 2009). The two RV(B) Tauri candidates fall within the relatively red re-

gion – their $V-I$ colors are 1.35 and 1.75 magnitudes, respectively – populated by the candidates for the SR variables, again consistent with their classification as radially pulsating supergiants (Samus et al. 2009). The $V-I$ colors of the candidates for eclipsing binaries are smaller than 0.77 magnitudes, and the absence of any red source supports the interpretation that in general the increased brightness of giants or supergiants makes it difficult to detect eclipsing dips. The B-band depth of their eclipsing dips changes between 0.130 and 1.080 magnitudes with an average of 0.494 magnitudes. The average is equivalent to ∼0.37 flux ratio, or mean radius ratio of ∼0.61 between the two stars in the binary system.

The 21 candidates for the unstudied type show a wide range of color ($V-I$ = 0.140–1.010 mag) similar to those of the Cepheid candidates. This, together with their B-band RMS variability of ∼0.026 magnitudes, indicates that some of the candidates for the unstudied type may be Cepheids with less convincing light curves. In Table 4 we summarize these candidates and their ranges of parameters for the different classifications.

Figure 9 shows a (B vs. $V-I$) color-magnitude diagram of the classified variable candidates. As above, we use the median magnitudes for each of BVI for the magnitudes and colors in the figure. While some types have clear color dependency, especially the red Mira and SR types as described above, all the types show a wide range of B-band magnitudes without any brightness dependency. For instance the differences in the B-band magnitudes among the Cepheid candidates are as large as five magnitudes. This implies that we are sampling these variable sources distributed through a large volume of space in the given line of sight.

5. Summary and Conclusion

We conduct analyses of 1247 variable sources found in a 20 square degree field in the direction of NGC 2784 as part of our KMTNet Supernova Program. Below are a summary and conclusion of our results.

- We identify 51 candidates for Cepheids, 17 for SR variables, 3 Mira types, 2 for RV(B) Tauri variables, 26 for eclipsing binaries, 1 active galactic nucleus, alongside 21 unstudied variables with rapid variability. This increases the sample sizes of some of these variable types known in this part of the Galaxy by a large margin, providing statistically important samples for further studies.
- Among the different types of the variables, we find that long-term variables, e.g., Mira types, are red in color and show large RMS variability. This supports the interpretation that substantial long-term variability is more prominent in the giant/supergiant phases of late-type stars.
- Our 26 candidates for eclipsing binaries appear to be color independent without any apparently red candidate, consistent with the expectation that their variability is due to geometrical configuration between two companions in a binary system. We measure the average depth of their eclipsing dips to be 0.494 magnitudes, and this is equivalent to 0.61 ratio in the relative sizes of the radii of the two members.
- Our results demonstrate the power of the KMTNet Supernova Program in studying variable objects of diverse types. The unique high-cadence, i.e., several exposures within 1-day cycle, long-term, multicolor monitoring of large fields with the three 1.6-m telescopes is capable of enabling unprecedented studies of variable objects. Of particular interests of future studies include the potential discovery of previously-unknown types of long-term variables and systematic investigation of some variable types, e.g., Cepheids, in the halo of the Galaxy.

Acknowledgments

This research was supported by the NSERC Discovery grant to DSM. This research has also made use of the KMTNet system operated by the Korea Astronomy and Space Science Institute (KASI) and the data were obtained at three host sites of CTIO in Chile, SAAO in South Africa, and SSO in Australia.

References

Christiansen, J. L., et al. 2008, The University of New South Wales Extrasolar Planet Search: a Catalogue of Variable Stars from Fields Observed between 2004 and 2007, MNRAS, 385, 1749

Cox, A. N. 1980, The Masses of Cepheids, ARAA, 18, 15

Cutri, R. M., et al. 2003, 2MASS All Sky Catalog of Point Sources, CDS/ADC Collection of Electronic Catalogues, 2246, 0

Freedman, W. L., & Madore, B. F. 2010, The Hubble Constant, ARAA, 48, 673

Freedman, W. L., et al. 2001, Final Results from the Hubble Space Telescope Key Project to Measure the Hubble Constant, ApJ, 553, 47

Hilditch, R. W. 2001, An Introduction to Close Binary Stars (Cambridge: Cambridge University Press)

Hubble, E. 1929, A Relation between Distance and Radial Velocity among Extra-Galactic Nebulae, PNAS, 15, 168

Jones, D. H., et al. 2009, The 6dF Galaxy Survey: Final Redshift Release (DR3) and Southern Large-Scale Structures, MNRAS, 399, 683

Karachentsev, I. D., Kaisina, E. I., & Makarov, D. I. 2014, Suites of Dwarfs Around Nearby Giant Galaxies, AJ, 147, 13

Kim, S.-L., Lee, C.-U., Park, B.-G., et al. 2016, KMTNet: A Network of 1.6 m Wide-Field Optical Telescopes Installed at Three Southern Observatories, JKAS, 49, 37

Leavitt, H. S., & Pickering, E. C. 1912, Periods of 25 Variable Stars in the Small Magellanic Cloud, HCOC, 173, 1

Malkov, O. Y., Oblak, E., Snegireva, E. A., & Torra, J. 2006, A Catalogue of Eclipsing Variables, A&A, 446, 785

Mandel, K., & Agol, E. 2002, Analytic Light Curves for Planetary Transit Searches, ApJ, 580, L171

Moon, D.-S., & Eikenberry, S. S. 2001a, QPO-Amplitude-Modulated Sidebands around Pulsational Frequency of LMC X-4 and Her X-1: Coupling between Periodic and Aperiodic Variability, ApJ, 549, L225

Moon, D.-S., & Eikenberry, S. S. 2001b, SMC X-1: A Flaring X-Ray Pulsar, ApJ, 552, L135
Moon, D.-S., Kim, S. C., Lee, J.-J., et al. 2016, Supernova and Optical Transient Observations Using the Three Wide-Field Telescope Array of the KMTNet, Proc. SPIE, 9906, 99064I
Neilson, H. R., & Ignace, R. 2014, Convection, Granulation, and Period Jitter in Classical Cepheids, A&A, 563, L4
Neilson, H. R., et al. 2012, Classical Cepheids Require Enhanced Mass Loss, ApJL, 760, L18
Park, H. S., Moon, D.-S., Zaritsky, D., et al. in preparation
Percy, J. R. 2007, Understanding Variable Stars (Cambridge: Cambridge University Press)
Perlmutter, S., et al. 1998, Discovery of a Supernova Explosion at Half the Age of the Universe, Nature, 391, 51
Riess, A. G., et al. 2016, A 2.4% Determination of the Local Value of the Hubble Constant, arXiv1604.01424
Samus, N. N., et al. 2003, An Electronic Version of the Second Volume of the General Catalogue of Variable Stars with Improved Coordinates, AstL, 29, 468
Samus, N. N., Durlevich, O. V., et al. 2009, General Catalogue of Variable Stars, VizieR Online Data Catalog, 1, 2025
Siebert, A., et al. 2011, The RAdial Velocity Experiment (RAVE): Third Data Release, AJ, 141, 187
Smith, H. A. 2013, Period Changes of Mira Variables, RR Lyrae Stars, and Type II Cepheids, arXiv1310.0533
Turner, D. G., Abdel-Sabour Abdel-Latif, M., & Berdnikov, L. N. 2006, Rate of Period Change as a Diagnostic of Cepheid Properties, PASP, 118, 410
Zacharias, N., et al. 2003, The Second U.S. Naval Observatory CCD Astrograph Catalog (UCAC2), CDS/ADC Collection of Electronic Catalogues, 1289, 0